UNIVERSITY OF MISKOLC
FACULTY OF MECHANICAL ENGINEERING AND INFORMATICS

INFLUENCE OF MANUFACTURING PARAMETERS ON PLA AND PLA–WOOD COMPOSITE MATERIALS: STATISTICAL, MACHINE LEARNING, AND BIOLOGICAL EVALUATION FOR BIOMEDICAL APPLICATIONS

Booklet of PhD Theses

Prepared by

Md Mazedur Rahman
Textile Engieering (BSc),
Mechanical Engineering (MSc)

ISTVÁN SÁLYI DOCTORAL SCHOOL OF MECHANICAL ENGINEERING SCIENCES
TOPIC FIELD OF DESIGN OF MACHINES AND STRUCTURES
TOPIC GROUP OF PRODUCT DEVELOPMENT AND DESIGN

HEAD OF DOCTORAL SCHOOL
Dr. Gabriella Bognár
DSc, Full Professor

HEAD OF TOPIC GROUP
DR. GABRIELLA BOGNÁR
SCIENTIFIC SUPERVISOR
Dr. SZÁVAI Szabolcs

Miskolc
2026

Judging Committee

Chair:

Secretary:

Members:

Official Reviewers

1. INTRODUCTION

Additive manufacturing (AM) is one of the most sustainable advanced manufacturing techniques, primarily depositing materials layer by layer to produce parts with improved characteristics such as better surface finish, lower manufacturing costs, reduced material waste, and desirable mechanical properties [1]. Therefore, this technique is currently adopted across multiple industries, including aerospace, construction, automotive, and biomedical sectors. [1].Moreover, the fabricated parts require a shorter manufacturing process compared to traditional or conventional manufacturing methods, including a wider scope for adopting various raw materials. In AM, additional benefits include the ability to produce intricate geometries, reduced carbon emissions, and potential energy savings[2].

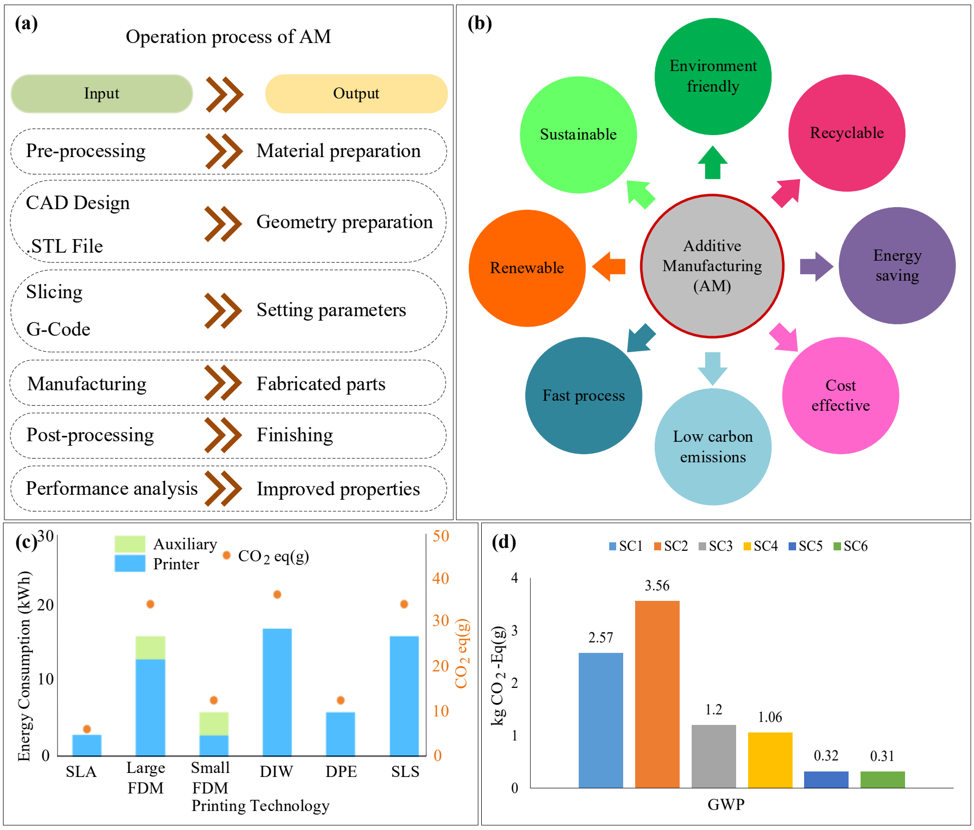

Figure 1: (a) Manufacturing processes of additive manufacturing (AM) methods; (b) benefits of AM methods [1], (c) energy consumption of different AM methods [3], (d) comparison of carbon dioxide emissions among different manufacturing methods [4].

Moreover, AM possesses several other highly demanded industrial features, including recyclability, renewability, biodegradability, cost-effectiveness, prolonged service life and environmental friendliness, making it superior to conventional manufacturing processes [5]. In particular to aerospace and automotive industries, the main goal is to reduce the weight of the materials with increased the machine and material overall efficiency which can be achieved through the AM or 3D/4D printing techniques [6]. However, in the biomedical industry, AM plays a significant role in designing prototypes of complex structures, which assists both researchers and industries in decision-making processes and, in some cases, is applied directly in real-life scenarios such as bio implantations [7]. Based on the type of raw materials or reinforcement materials and manufacturing processes, the AM or 3D printing methods are classified as material extrusion (ME), vat polymerization (VP), material jetting (MJ), sheet lamination (SL), powder bed fusion (PBF), direct energy deposition (DED), binder jetting (BJ), Cold Spray Additive Manufacturing, and additive friction stir deposition [7]. In most cases, the manufacturing process follows a similar process flow. Initially, a 3D CAD model is created using specialized design software [8]. The model is then converted into an STL file format, which defines the surface geometry of the part. This STL file is subsequently imported into slicing software, where it is digitally divided into layers and the corresponding G-code is generated. The slicing software also enables the configuration of key manufacturing parameters such as layer thickness, print speed, and infill density. Finally, the generated G-code is transferred to the 3D printing machine, which fabricates the component layer by layer to produce the final part. The manufacturing processes of additive manufacturing (AM) methods are illustrated in Figures 1(a) and 1(b). In contrast, Figures 1(c) and 1(d) depict the energy consumption and carbon dioxide emissions associated with various AM methods and conventional manufacturing techniques.

Considering these outstanding advantages, the adoption of AM or 3D/4D printing has significantly increased in modern industries. One study reported that the market size of the U.S. AM industry was approximately USD 3.56 million in 2022, and it is projected to grow at a compound annual growth rate (CAGR) of 21.3% from 2023 to 2030. Furthermore, the analysis revealed that this method supports the production of software, hardware, and related services, with hardware alone accounting for more than 64.1% of the total revenue share in 2022[9]. However, a recent study highlighted that the market revenue of additive manufacturing (AM) in the U.S. market was USD 17.99 billion in 2024, and it is projected to increase linearly to USD 110.13 billion, with a compound annual growth rate (CAGR) of 19.83%, as depicted in Figures 2 (a) and 2 (b). The study further indicated the market share by region as follows: North America – 36.14%, Europe – 30.40%, Asia-Pacific – 26.41%, Latin America – 5.02%, and the Middle East and Africa – 2.03%[10], as shown in Figure 2(c). Figure 2(d) presents the market share distribution of different types of 3D printers, including industrial and desktop systems. In addition, the adoption of AM or 3D printing contributes to reducing carbon dioxide emissions, which are typically produced through conventional manufacturing processes. For example, one study highlighted that AM can reduce carbon dioxide emissions by up to 70% in the building and construction industries. Notably, the AM market has shown significant growth in healthcare and biomedical industries. According to the study, the market value of AM in the U.S. healthcare sector was USD 7.4 billion in 2022 and is expected to reach approximately USD 27.3 billion by 2030[9]. The analysis further indicated that the market's CAGR would be 18.1%, with key applications in medical implants, prosthetics, wearable devices, tissue engineering, dental applications, and other related fields, as depicted in Figure 3 (a).

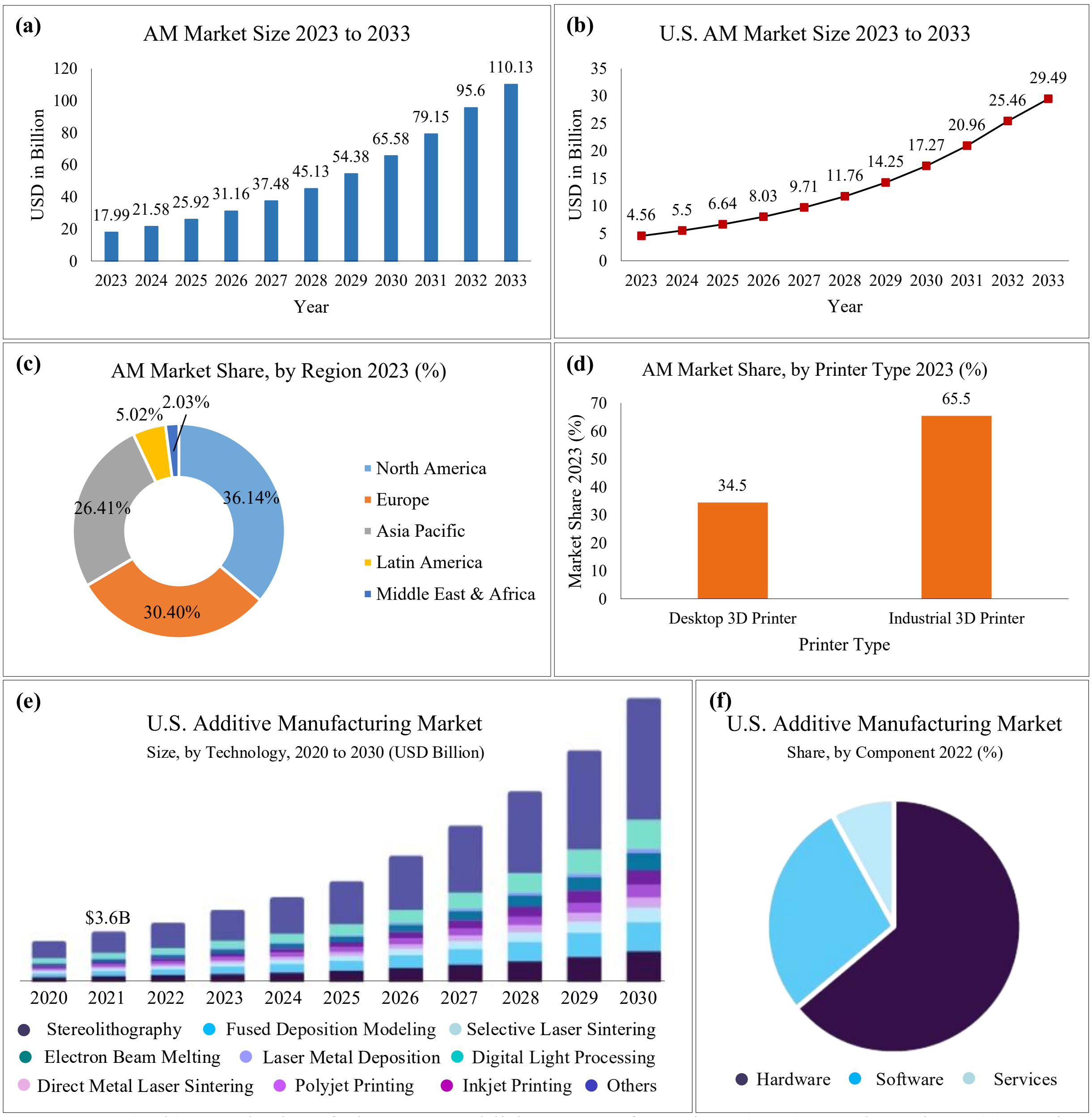

Figure 2: (a–b) Analysis of the U.S. additive manufacturing (AM) market size; (c) regional distribution of the AM market share in 2023; (d) AM market share in 2023 based on different types of 3D printers[10], (e) projected U.S. AM market trends based on different manufacturing methods, and (f) U.S. market shares of AM-fabricated hardware, software, and services[9].

Moreover, the study demonstrated that the market value of polymers in AM is considerably higher compared to metals, biological cells, and other materials, presented in Figure 3 (b). Reducing carbon dioxide emissions and energy consumption in manufacturing processes has become one of the major priorities of modern industries, as most manufacturing operations are directly or indirectly associated with carbon emissions throughout their production stages [1].

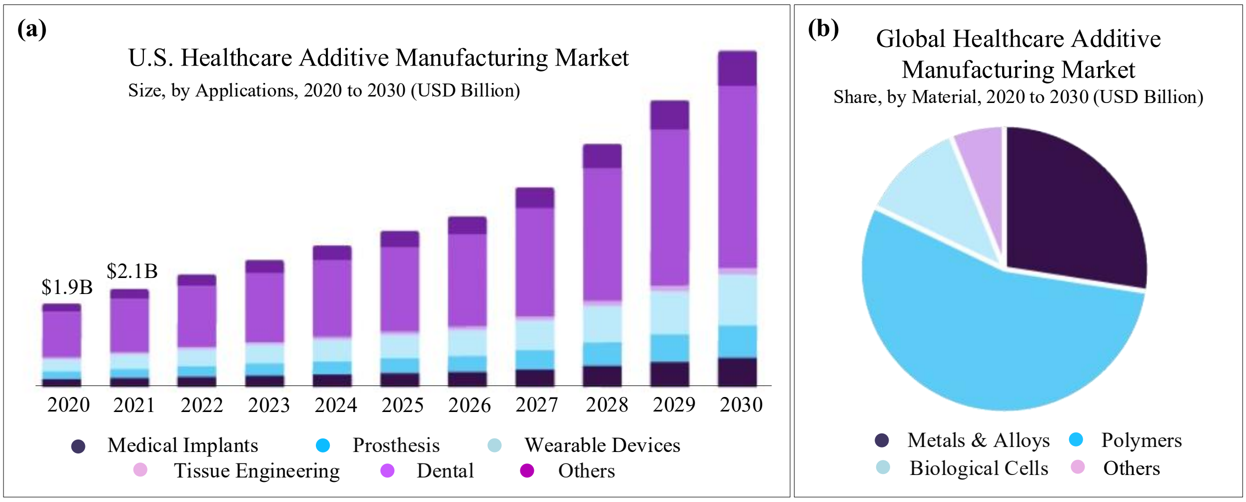

Figure 3: (a) U.S. additive manufacturing (AM) market size in biomedical industries and (b) global market size of AM-fabricated metals, polymers, and biological cells based on different material types[9].

In the aviation industry alone, approximately 3% of global greenhouse gas emissions originate from this sector, and this figure is expected to increase by 300–500% by 2050. However, this can be drastically reduced through the adoption of 3D/4D printing technologies in various applications[11] . Compared to traditional manufacturing processes, additive manufacturing (AM) or 3D/4D printing can produce the desired components with significantly lower carbon emissions and energy consumption. A comparative study analyzed the environmental impacts of a 3D-printed part versus a conventionally manufactured one [4]. The findings revealed that replacing conventional manufacturing machines with industrial-scale 3D printers can reduce global warming potential by about 88%, decrease carbon emissions by 94%, and improve energy efficiency and material utilization through waste reduction and enhanced performance. Similarly, another study compared different 3D printing methods used in pharmaceutical applications and found that most 3D printers produced less than 120 g CO_2-eq per 10 units—substantially lower than conventionally manufactured alternatives [3]. Furthermore, specific examples of carbon emission reductions have been reported in the construction industry. One investigation found that adopting 3D printing technology could potentially reduce carbon emissions by approximately 16.16% compared to conventional manufacturing processes in construction [12]. Regarding energy consumption, it varies depending on the 3D printing process and selected parameters, although it generally remains more efficient than traditional methods. For instance, a study on fused deposition modeling (FDM) revealed that higher layer thickness, higher printing speeds, and lower bed temperatures significantly reduced total energy consumption. The study further concluded that bed temperature alone accounted for 60–70% of the total energy use in FDM 3D printing [13].

Lattices are a class of cellular structures intentionally designed with voids to enhance the overall efficiency of materials by reducing weight, decreasing manufacturing costs, and maintaining desired mechanical performance compared to conventional solid structures used in various domains [14,15]. Although the primary objective of lattice structures is to improve load-bearing capacity in different applications, it is important to note that variations in lattice geometry, material type, and fabrication processes can result in different mechanical and functional responses. The selection of lattice configuration and material type largely depends on the intended application. In biomedical applications, materials such as ceramics, metals, polymers, hydrogels, and their composites or hybrid composites are widely employed for the fabrication of lattice structures [16]. Lattices are generally classified based on their porosity characteristics and unit cell orientation [16]. Specifically, in tissue engineering and bone scaffold applications, unit cell–based lattice structures are predominantly adopted due to their ability to mimic natural bone architecture. Among all available fabrication techniques, additively manufactured lattice structures are considered more suitable for biomedical applications because of their superior design flexibility, smooth surface finish, and simplified material handling compared to conventionally manufactured counterparts [17]. However, there are several limitations associated with additively manufactured lattice structures. These include insufficient mechanical strength, the need for extensive post-processing, potential material toxicity, and the requirement for complex equipment and support structures during fabrication [18]. Moreover, not all materials used in AM are approved under global standards such as those established by the U.S. Food and Drug Administration (FDA). In evaluating the performance of lattice structures, key parameters such as compressive strength, biocompatibility, biocorrosion, and biodegradation are critically assessed before their consideration for real-life biomedical applications such as bio implantations[18]. In biomedical tissue engineering applications, scaffolds are defined as three-dimensional frameworks that facilitate cell attachment, proliferation, and migration, while maintaining biocompatibility and supporting tissue regeneration and integration in vivo [19]. The main distinction between a scaffold and a lattice structure lies in their primary functions: the lattice represents the architectural component within the scaffold that plays a crucial role in tailoring its mechanical properties, including porosity, permeability, and bio-integration performance [20]. In essence, the lattice provides the engineering support, whereas the scaffold delivers the biological functionality. In scaffold design, biological performance is strongly influenced by the surface area-to-volume ratio and the geometric configuration of the internal lattice structure, which collectively determine the extent of cell–material interactions and biological responses [21]. In particular, bone tissue scaffolds are designed to enhance patient recovery by reducing pain, restoring functional capacity, and promoting new bone and cell growth within damaged regions [22]. It is important to note that the mechanical performance of a scaffold such as its load-bearing strength—is not directly responsible for cell proliferation or tissue generation. Instead, its primary role is to provide structural support to withstand physiological loads, thereby maintaining mechanical stability until new tissue formation occurs. Consequently, mechanical characterization often precedes biological assessment in scaffold evaluation, particularly for applications focused on bone and tissue engineering.

Composite materials are defined as materials in which certain fibers or particles are reinforced within a specific matrix in a particular proportion. In the case of hybrid composite materials, the types of reinforcing fibers can vary and are often more diverse than those used in traditional composites. The primary objective of developing composite materials is to achieve a combination of desirable mechanical and functional properties, such as improved load-carrying capacity, high strength, and enhanced strength-to-weight ratio [1] . In biomedical applications, composite materials are widely utilized for bone replacement, spinal and joint implants, and various other medical applications [23]. Hybrid composites, in particular, are often more advanced than conventional composites, offering superior mechanical and biological performance. In some cases, hybrid composites have demonstrated elastic modulus and strength values comparable to those of natural bone, as reported in recent studies [24]. Both conventional and hybrid composites can be fabricated from a wide range of materials—such as polymers, natural fibers, metals, ceramics, minerals, and hydrogels—depending on the specific application and intended purpose. The primary focus in biomedical fabrication lies in achieving biocompatibility and other favorable biological responses necessary for successful bio implantation. In addition to traditional additive manufacturing (AM) processes, recent research has explored innovative approaches, such as incorporating nanomaterials into fabricated parts. For example, one study fabricated a lattice scaffold from extracted cellulose reinforced with nano-hydroxyapatite (n-HAP) using an extrusion-based AM method and reported excellent biological responses, suggesting its potential for tissue engineering applications [25]. Despite these promising outcomes, several challenges can arise during the fabrication and application of AM-based lattice composite bioimplants. Improper composite formulation may lead to poor cell adhesion and impaired osseointegration, resulting in weak bonding between the lattice and surrounding tissues [26]. Furthermore, stress-shielding effects may occur if the AM-fabricated composites are composed of excessively strong or dense materials. Long-term complications can also develop after implantation, such as wear, corrosion, fibrous encapsulation, inflammation, and reduced fracture toughness. Over time, these issues may lead to cracking or failure of the implant, necessitating revision surgery. Such complications can result in prolonged recovery times, increased medical costs, and, in severe cases, fatal outcomes [26]. To overcome these challenges, further biomechanical and biological performance evaluations are required through extensive experimental trials before real-life applications or bio implantations are undertaken[27].

In material extrusion, Fused Deposition Modelling (FDM) or Fused Filament Fabrication (FFF) has become increasingly popular for fabricating lattice composite structures due to its low manufacturing cost, simpler processing, wide range of available biopolymers and composite filaments, and its environmentally friendly and energy-efficient nature[8]. Before fabricating lattice composite scaffolds, the filaments are first produced as composite formulations. For example, an extruder—either twin-screw or single-screw—is used to fabricate the filaments, where a hopper feeds the filament matrix pellets along with the desired composite powders or pellets[1,28]. Among the extrusion processes, nanoparticles are added to enhance the mechanical properties and achieve the desired performance of the lattice composite scaffolds [29]. After obtaining the filaments, they are fed into an FDM 3D printer to further fabricate the lattice composites.

FDM can be applied in multiple areas of the biomedical industry, particularly in bone defect repair, bone regeneration, osteogenesis, tissue engineering, and other related applications. For example, this research used polyetheretherketone (PEEK) incorporated with calcium hydroxyapatite (cHAp) to fabricate a lattice composite scaffold, which showed significant in vitro results and was further proposed for potential applications in bone defect repair through implantation [29]. Similarly, this study fabricated a polylactic acid (PLA) composite incorporating magnesium (Mg) and nano-hydroxyapatite (n-HA) and investigated the in vitro and in vivo outcomes of FDM-printed composite scaffolds. In the in vitro experiments, the biocompatibility, osteogenic properties, and angiogenic capabilities were evaluated, while the in vivo studies explored the underlying pathways of osteogenesis and angiogenesis. The results indicated that the 10% Mg composite exhibited optimal osteogenic properties, whereas the 20% Mg composite showed superior angiogenic effects. In terms of mechanical performance, the highest compressive modulus (200–210 MPa) was achieved at 10% Mg content. Although the addition of Mg slightly reduced the overall modulus, the study concluded that the proposed composite scaffold is a promising candidate for treating critical-size trabecular bone defects, as it demonstrated favorable outcomes in animal trials [30].

2. METHODOLOGY OF THE STUDY

In this section, the overall methodology for the lattice composite is presented, covering the design, fabrication, and experimental processes. The method includes finite element method (FEM) analysis, modeling, fabrication, data analysis, machine learning, and other related processes. Moreover, the necessary precautions, along with the biological evalua-tions, are discussed in detail in accordance with ASTM and ISO standards. Each stage is de-scribed in the following sections.

2.1. Research methodology for FEM investigations on different lattice structures

To optimize and understand the performance of different strut diameters, filament types, and lattice structures, finite element method (FEM) analysis was first conducted. Three different polymeric materials such as PLA, ABS and nylon filaments are considered to calculate the compressive behavior of different lattices and their struts. The isotropic properties of all filaments are listed in Table 1. The material properties of the considered polymeric materials are taken from the literature[31,32].

Table 1: Isotropic material properties of PLA,ABS, and nylon.

Material	**Young's modulus (GPa)**	**Poisson's ratio**	**Density (g/cm3)**
PLA	3.5	0.38	1.25
Nylon 618	2.95	0.36	1.10
ABS	0.862	0.35	0.78

A design of experiment (DOE) was developed using a software called Minitab-19 to investigate the compressive behavior on three different lattice structures, filaments and strut diameters. The design is based on Taguchi L9 orthogonal array. The DOE has been presented in Table 2.

Table 2: Design of the experiment in L9 orthogonal array.

Factor	**Name**	**Level values**	**Column**	**Level**
A	Strut diameter	1.0 1.5 2.0	1	3
B	Filament type	PLA ABS Nylon	2	3
C	Lattice type	SC SC-BCC FCC	3	3

The finite element investigations were conducted using the ABAQUS software. The validity of this work is checked by comparing with the literature [33], where two types of simple cubic (SC) unit cells (1,27 cell numbers) with Ti-6Al-4V alloy material are considered. The material properties are defined as elastic-plastic in behavior by the Johnson-Cook material model. However, it should be noted that the increment steps are 15 for the analysis. From the analysis and comparison, it is evident that the results obtained by FEM and other literature outcomes are compatible with each other. The stress-strain curve with comparison is presented in **Figure 4** (a) and Figure 4 (b) below. The deviation between the reference study and the current research was less than 5%.

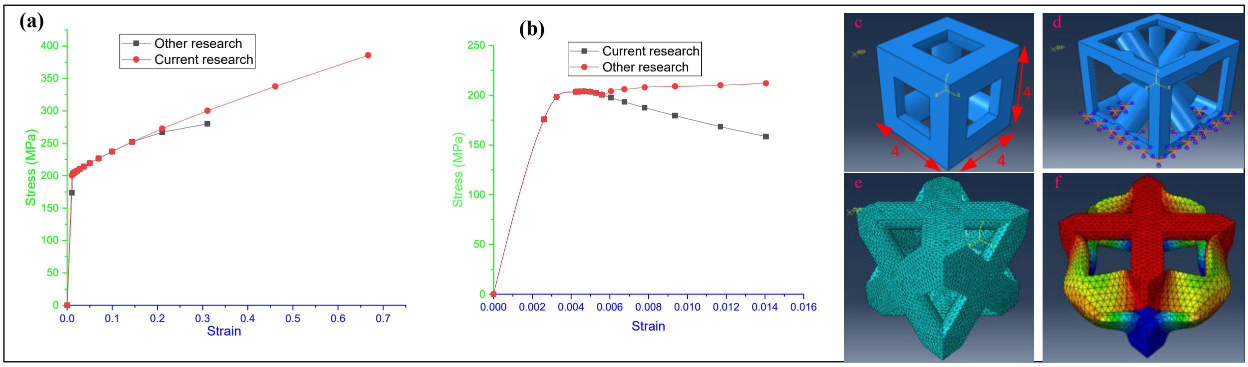

Figure 4: (a) Stress-strain curve comparison with current research outcomes and other literature outcomes[33]for unit cell 27, (b) Stress-strain curve comparison with current research outcomes and other literature outcomes[33] for unit cell 1, (c) SC lattice at 2 mm strut diameter, (d) SC-BCC lattice at 1.0 mm strut diameter with implemented boundary conditions, (e) FCC lattice structure at 1.5 mm strut diameter with tetrahedral mesh, (f) FCC lattice structure's deformation pattern after compression test.

First, the lattice unit cell has been designed according to DOE's strut diameter. Since, the number of unit cell does not play a significant role in computing the mechanical properties [33], therefore, we considered a unit cell in this study. The overall dimension in the unit cell is 4 mm x 4 mm x 4 mm. After that, the material properties are assigned to the unit cell and a tetrahedral mesh is created in the unit cell. The boundary and loading conditions need to be defined in the lattice cell before conducting the compression test. Hence, three sets are created at the bottom, top and a reference point of the lattice structure to define the boundary and loading conditions.

However, the reference point is defined at the (0,4,5) point to create a gap between the loading point and the lattice structure. Later on, the bottom section is fixed in all directions and load is generated from the Y direction of the reference point. An earlier study found that different compression speeds have a significant role in the outcomes[34], therefore in this study the compression speed is considered as 1.5 mm/min which is suitable for polymer type materials[35]. The incrementation in the loading step is 15. Before submitting the simulation, a constraint equation has been created which is defined in the top sets and reference point set. The force-displacement curve has been plotted from the reference point. The finite element set up is demonstrated in **Figure 4** (c-f).

2.2. Research method for PLA simple cubic lattice scaffold investigations

The material used in this research is a commercial PLA filament with a diameter of 1.75 mm. The material was purchased from Creality (Shenzhen, P.R. China). Compared to other lattice structures such as body centered cubic, and face centered cubic, simple cubic lattice structure provides better mechanical performance[33]. Therefore, this research considers a simple cubic lattice structure. Firstly, a CAD model is designed in a commercial CAD software with a dimension of 36.0 mm × 36.0 mm × 30.21 mm to conduct the compression test (according to ASTM D695) [36] and evaluate the mechanical properties.

The design of the experiment (DOE) has been performed through Minitab 19. For Taguchi selection, 4 level design has been opted, considering four significant printing parameters such as layer height, printing temperatures, printing speed, and bed temperatures. The levels were chosen based on the manufacturer's instruction and existing literature. Finally, the L_{16} orthogonal array has been employed to design the DOE. DOE is presented in detail in **Table 3**.

Table 3: Taguchi L_{16} Experimental design (DOE).

DOE SL.	**Layer height (mm)**	**Printing temperature (°C)**	**Printing speed (mm/s)**	**Bed temperature (°C)**
E-1	0.1	195	30	50
E-2	0.1	200	40	55
E-3	0.1	205	50	60
E-4	0.1	210	60	65
E-5	0.15	195	40	60
E-6	0.15	200	30	65
E-7	0.15	205	60	50
E-8	0.15	210	50	55
E-9	0.2	195	50	65
E-10	0.2	200	60	60
E-11	0.2	205	30	55
E-12	0.2	210	40	50
E-13	0.25	195	60	55
E-14	0.25	200	50	50
E-15	0.25	205	40	65
E-16	0.25	210	30	60

To fabricate the design on the FDM 3D printing machine, the model has been introduced with an available slicer software named Creality Slicer. After combining all the input parameters from the DOE into the slicing software, the software provides a predicted production time with a G-code. Later on, the obtained G-code was inserted into the FDM printing machine using a memory card. During fabrication, some crucial factors, such as the dimension of the lattice structure and strut diameter, have been scrutinized. In addition, PLA filament can be significantly affected by moisture content and humidity [37,38]; therefore, this study considers some precautions, such as using a polyethylene bag to put the sample after fabrication, and checking the dimension measurements against CAD modeling for printing accuracy., as shown in **Figure 5** (b) . However, other parameters, like the infill density of 100%, shell thickness of 1.2mm, flow rate of 100%, and the nozzle size of 0.4mm are kept constant during printing.

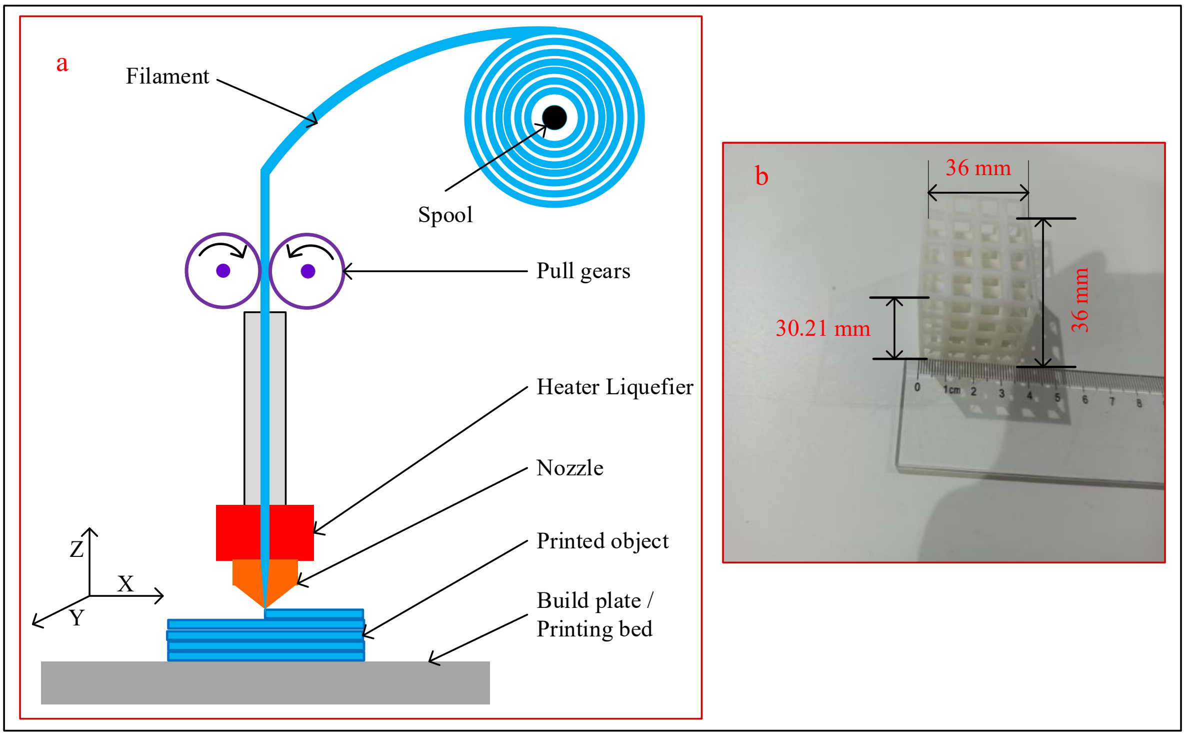

Figure 5 (a) A schematic process of lattice cube printing on FDM 3D printer, **(b)** lattice dimension measurement.

The compression test has been conducted (according to ASTM-D695) on a SENS universal testing machine (model CMT-6000) with a compression speed of 2 mm/min and a 10 KN load cell. An earlier study found that different compression speeds can remarkably influence mechanical properties [39]. To achieve better outcomes, this study considered 2mm/min speed, which has been obtained from other literatures of PLA materials[31,40,41] . Likewise, to get accurate results, five samples are tested of each consideration (from DOE). The preload between platens and samples is 0-5N for all tests. The accuracy of this universal testing machine is ±0.5%.

On the other hand, SEM test has been conducted on a JSM7800F (origin-Japan) machine. First, the sample is cut with scissors, and a specific size is taken from different regions of the sample. After that, the sample was attached to the sample plate by using conductive glue. Before conducting the test, all samples were dried and sputtered with gold in a sputtering machine. Each sample sputtered 4 times (a total of 120 seconds). It is important to note that the conductive glue and spraying gold are used to increase the conductivity of the sample surface. The thickness of the coating was approximately 2-3 nanometers (nm). Later on, the sample plate was placed in the sample chamber. Finally, SEM photos of different samples have been collected at 5.0 Kilo Volt (KV) and secondary electron mode with different magnifications.

2.3. Research method for wood-PLA simple cubic lattice scaffold investigations

2.3.1. Wood-PLA lattice scaffold fabrication, mechanical, physical and biological process

In this research, also a wood–PLA composite containing 10% wood particles was used. The wood–PLA filament was commercially purchased from Qidi, a manufacturer of filaments for FDM 3D printing [42]. Although various types of commercial wood–PLA filaments are available, a 10% wood content was selected for this study because this proportions are more suitable for NFRCs based composite. A comparative study evaluated the effect of wood content ranging from 0% to 50% in PLA composites, focusing on tensile strength [43]. The results revealed that the highest tensile strength (57 MPa) was obtained at 10% wood content. As the wood proportion increased, both tensile strength and elastic modulus decreased linearly. This reduction may be attributed to increased brittleness at higher wood loadings, leading to earlier collapse or failure of the material. Furthermore, the lowest tensile strength (30 MPa) was observed at 50% wood content. However, in terms of dimensional stability, the 10% wood–PLA composite exhibits slight deviations in moisture absorption and thickness swelling ratio compared with pure PLA [44]. Nevertheless, due to the relatively low wood content, the dimensional changes in the printed parts remain limited and do not significantly affect their structural stability. The density of the considered wood–PLA filament for this study ranged from 1.22 to 1.24 g/cm^3 [42].

The design of the experiment was developed using the statistical analysis software Design-Expert (Version 13). Four critical input parameters were considered: layer height, nozzle temperature, printing speed, and infill density. Previous studies have indicated that, for NFRC-based composites, lower layer heights, lower nozzle temperatures, and moderate to high infill densities are generally more suitable for FDM-fabricated parts[28]. However, these variables do not always produce consistent outcomes, as the results may vary depending on the geometry and structural configuration of the printed components. Therefore, the selected parameter ranges were determined based on existing literature and the manufacturer's recommended settings [28,42]. A Central Composite Design (CCD) was employed to structure the experimental plan. The design consisted of 30 experimental runs, including 24 unique design points and 6 replicates at the center points. The detailed design matrix is presented in **Table 4.**

Table 4: Experimental design matrix for the wood–PLA lattice composite prepared using Central Composite Design (CCD).

Input variables	Low level	High level
Layer height (mm)	0.1 mm	0.3 mm
Printing speed (mm/s)	40 mm/s	60 mm/s
Nozzle temperature (°C)	195°C	215°C
Infill density (%)	70%	100%

Apart from these variables, several additional printing parameters were kept constant throughout the investigation, as previous studies have indicated that they do not have a significant influence on the measured outcomes. These fixed parameters are listed in **Table 5.**

Table 5: Constant process parameters used in the FDM 3D printing machine.

Constant parameters	Values
Infill pattern	Cubic
Travel speed	100 mm/s
Build plate temperature	60 °C
Fan speed	100%
Z offset	0.0 mm
Top layers and bottom layers	4

The samples for the wood-PLA lattice scaffold were designed similarly like PLA lattice. The specimens were fabricated using an FDM (Fused Deposition Modeling) 3D printer (QIDI brand, model QIDI Max 4) with a build volume of 390 × 390 × 340 mm^3 and a nozzle size of 0.4 mm. During fabrication, nozzle clogging was encountered due to the use of natural fiber-reinforced wood–PLA filament. To mitigate this issue, the nozzle was thoroughly cleaned before and after each fabrication process**. Figure 6(a)** illustrates the FDM fabrication process, while **Figure 6(b)** presents the fabricated wood–PLA composite lattice structure.

The primary objective of this research was to investigate the compressive behavior of the wood–PLA composite lattice. Compression testing was performed using an MTS 322 test frame with a maximum load capacity of 100 kN. The loading rate can significantly influence the mechanical response of lattice structures. To ensure consistency and avoid unintended variations in the results, a crosshead speed of 2 mm/min was selected, following previously reported studies [45,46].

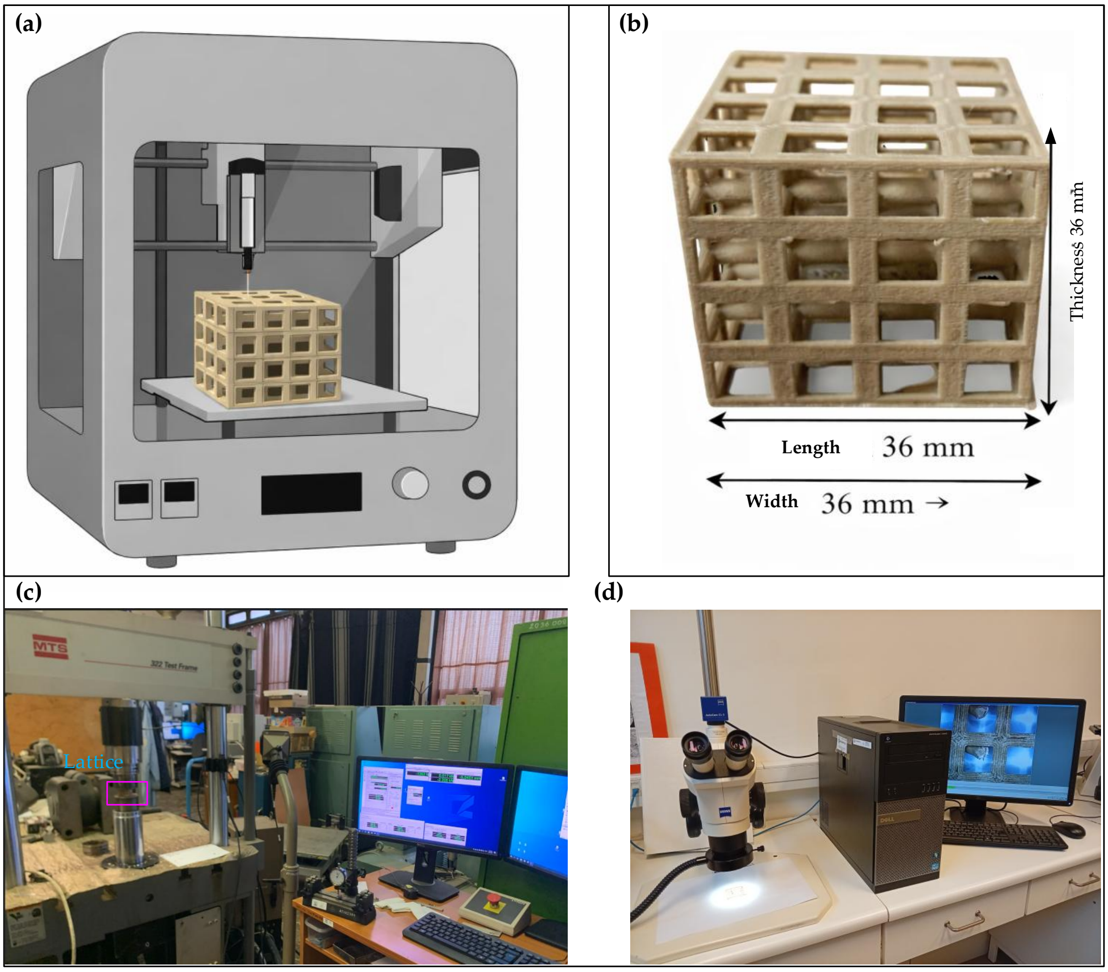

Figure 6: (a) Fabrication process of the FDM 3D-printed wood–PLA composite lattice; (b) fabricated lattice structure with dimensions; (c) compression test setup using the MTS 322 Test Frame universal testing machine; (d) microscopic examination setup using the Zeiss Stemi 2000-C.

Furthermore, to improve the accuracy and reliability of the experimental results, the compression displacement was limited to 22 mm. Beyond this displacement, the lattice structure exhibited densification behavior, effectively transforming into a sandwich-like compact structure and demonstrating artificially elevated compressive strength. Therefore, restricting the compression bar travel ensured that the results reflected the intrinsic compressive performance of the lattice structure prior to full densification. The compression test setup is illustrated in **Figure 6(c).**

Finally, to compare the mechanical performance within the designed DOE framework, the fracture regions of the wood–PLA lattice composites were examined using a microscope, as shown in **Figure 6(d).** The microscope used in this study was a Zeiss Stemi 2000-C model. The fractured surfaces were analyzed at different magnifications to evaluate the failure modes and crack propagation characteristics.

After conducting the compression test, the load–displacement curve was obtained for each experimental design. The load values were then converted into stress by dividing by the surface area. The total surface area was 1296 mm². However, the void section was excluded by subtracting 577 mm² from the original area. Therefore, the effective cross-sectional area of the lattice was taken as 719 mm², which was used to calculate the stress of the wood–PLA composite lattice. The effective cross-sectional area mainly represents the mechanical properties of lattice-type structures, as reported in earlier studies [8,47,48].

To evaluate and understand the compressive behavior of the wood–PLA lattice composite, two key responses were considered: compressive strength and compressive modulus. These responses were determined for each DOE specimen based on its corresponding stress–strain curve. Previous studies have shown that higher values of compressive strength and compressive modulus indicate a stronger and stiffer material or structure compared to those with lower values[8]. The compressive strength and compressive modulus reported in this study represent the average of three experiments, conducted to minimize experimental errors and improve the accuracy and reliability of the overall investigation.

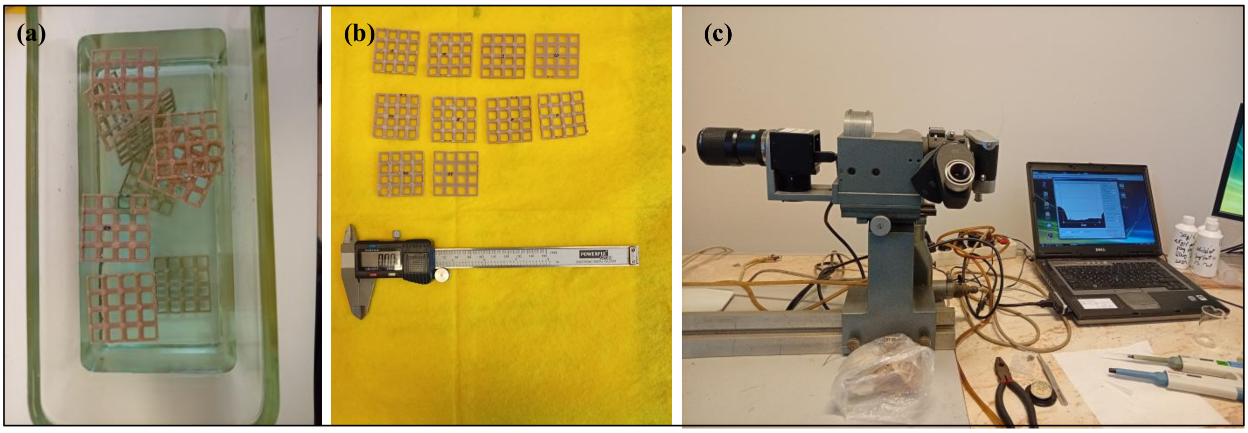

Figure 7: (a) Prepared lattice samples for the water absorption experiment, (b) water absorption and thickness swelling measurements (%) after 24 h and 48 h, and (c) experimental setup for the contact angle measurement.

Water absorption and thickness swelling tests were conducted following ASTM D570, with slight modifications due to the lattice geometry of the specimens, similar to the procedure reported in the literature [49]. The lattice samples were immersed in distilled water, and the changes in mass and thickness were recorded after 24 h and 48 h of immersion as depicted in **Figure** 7 (a) and (b). To ensure accurate thickness swelling measurements, a reference point was marked on the specimen using a permanent marker so that the same location could be measured after 24 h and 48 h. For the surface wettability analysis, the static contact angle was measured using the sessile drop method according to ISO 19403-2:2024, similar to the approach described in previous research [50]. A 10 μL droplet of distilled water was deposited on the surface of the lattice specimens due to their thin-wall structure. After 30 s, the droplet images were captured using a microscopic imaging system illustrated in **Figure 7** (c). The captured images were analyzed using KSV CAM software (version 2008) to determine the contact angle. The baseline was carefully fitted to the sample surface to obtain accurate measurements. For each specimen, three contact angle measurements were taken at different locations, and the average value was reported. Prior to testing, the samples were dried and conditioned at 23 °C and handled carefully during the measurements to ensure reliable and consistent results.

Scanning electron microscopy (SEM) analysis was performed using a ZEISS EVO 10 MA SEM equipped with an EDAX Genesis Apex2 energy-dispersive X-ray spectroscopy (EDS) detector. The fracture regions and selected parts of the lattice structures were carefully considered, cut, and mounted onto the sample holder using conductive carbon cement. Prior to observation, a thin conductive gold coating was applied using a sputter coater to prevent surface charging during imaging. SEM examinations were conducted under high vacuum conditions with an accelerating voltage of 10 kV for the original surfaces and 20 kV for the fracture surfaces. The beam current was maintained at 0.4 nA during the analysis.

In order to assess the cytocompatibility of the 3D-printed wood–PLA lattice structures, a cell viability test using the Neutral Red uptake assay was performed. The human buccal carcinoma cell line TR-146 (ECACC No: 10032305, passage number 25) was seeded into a 96-well plate at a density of 1×10^4 cells per well in Dulbecco's Modified Eagle Medium (DMEM) supplemented with cell culture additives (10% (v/v) fetal bovine serum (FBS), 3.7 g/L sodium hydrogen carbonate, 1% (v/v) non-essential amino acid solution, 100 IU/mL penicillin, and 100 μg/mL streptomycin sulphate). The cells were incubated for 7 days at 37 ± 1 °C in a humidified atmosphere containing 5% CO_2 to allow cell attachment and growth. Fragments of the 3D-printed structures were incubated in cell culture medium for 7 days at 37 ± 1 °C to prepare the material extracts. Three extract concentrations (16.6 mg/mL, 50 mg/mL, and 100 mg/mL) were prepared, and 200 μL of each extract-containing medium was added to the cells in the 96-well plate (12 wells per treatment group) after removing the original culture medium. The cells were exposed to the extracts for 24 h. After the treatment period, the medium was removed and 200 μL of Neutral Red solution (33.3 μg/mL Neutral Red dye in culture medium) was added to each well, followed by incubation for 2 h. Subsequently, the dye-containing medium was removed and 100 μL of a desorption solution consisting of isopropanol and 1 M hydrochloric acid (25:1) was added to each well to dissolve the incorporated dye. The absorbance of the extracted dye was measured at 540 nm using a Thermo Fisher Multiskan Go microplate reader (Thermo Fisher Scientific, USA). Wells without cells were used as blanks. The cell viability values were expressed as mean ± standard deviation (SD) relative to the untreated control cells containing only culture medium [51].

2.3.2. Machine Learning Modelling

In this research, machine learning (ML) models were employed as an efficient predictive tool to reduce reliance on destructive experimental testing and computationally expensive, time-consuming numerical simulations. Traditional experimental and finite element analyses, although accurate, require significant material preparation, testing time, and computational resources. By learning the relationship between printing parameters and the corresponding compressive strength and compressive modulus response from a limited set of experimental data, the developed ML models enable rapid and reliable prediction for new configurations.

The dataset constructed for machine learning prediction for this study was derived from 24 unique specimen configurations, each tracked via a unique specimen ID. The experimental stress-strain data for each specimen was uniformly sampled to yield 500 discrete points per curve. Consequently, a comprehensive dataset comprising 12,000 rows and 6 columns was generated. For the development of the predictive model, stress was defined as the target feature, while layer height, printing speed, nozzle temperature, infill density, and strain served as the input features. **Table 6** represents the dataset used for this study.

Table 6. Dataset for Machine Learning modelling

Specimen_ID	Layer height, mm	Printing speed, mm/s	Nozzle temperature (℃)	Infill density (%)	Strain	Stress
1	0.2	50	185	85	0	0.018539
1	0.2	50	185	85	0.000159	0.019113
1	0.2	50	185	85	0.000318	0.019687
.	.	.	.	.	.	.
.	.	.	.	.	.	.
.	.	.	.	.	.	.
.	.	.	.	.	.	.
24	0.3	40	215	70	0.081526	2.617483
24	0.3	40	215	70	0.081689	2.614002

The models utilized in this work are based on ensemble learning techniques. The fundamental principle of ensemble learning is to employ more than one learner and integrate their predictions to form a single model that is stronger and more accurate than any individual learner. By combining multiple models, ensemble learning improves predictive performance, robustness, and generalization capability. This framework includes several methodologies, among which bagging and boosting are the most prominent. Boosting is a major ensemble learning technique and is regarded as one of the most powerful learning methods, forming the foundation of advanced algorithms such as XGBoost, LightGBM, and CatBoost [52]. In this research only the XGBoost model is used.

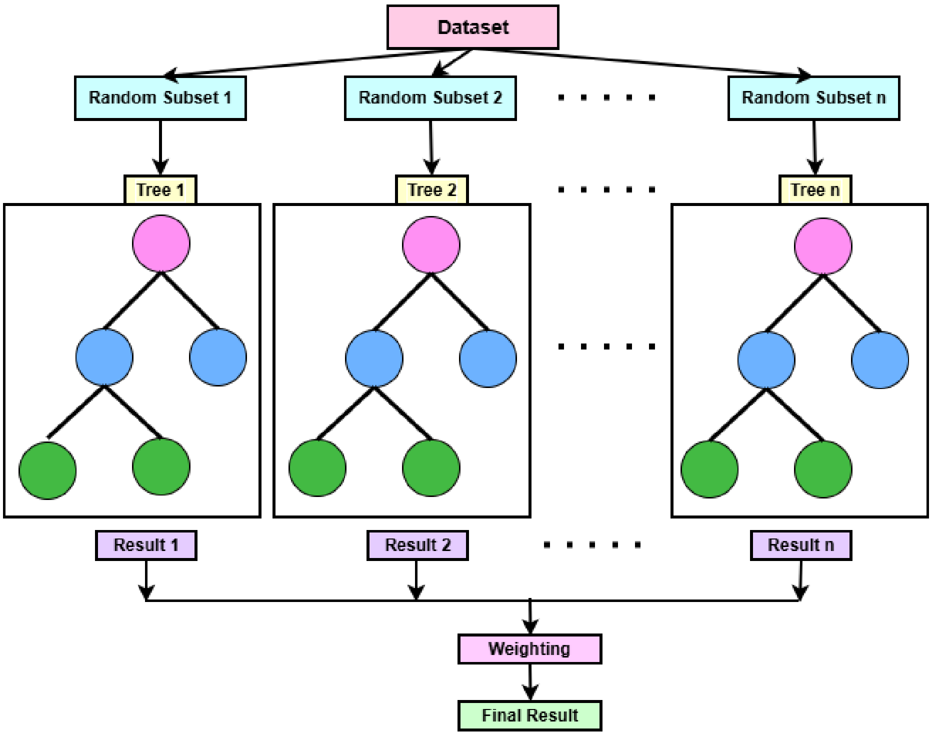

Figure 8: XGBoost Algorithm [53].

Root mean squared error (RMSE) measures the square root of the average squared differences between predicted and observed values, thereby assigning greater weight to larger prediction errors and emphasizing model sensitivity to significant deviations. Eq. (1) represents the numerical formulation of RMSE.

$$RMSE = \sqrt{\frac{1}{n}\sum_{i=1}^{n} (y_i - \hat{y_i})^2} \tag{1}$$

Mean absolute error (MAE) computes the average absolute difference between predicted and observed values, providing an intuitive and easily interpretable measure of overall model prediction accuracy. Eq. (2) is the numerical equation of MAE.

$$MAE = \frac{1}{n}\sum_{i=1}^{n} |y_i - \hat{y_i}| \tag{2}$$

Coefficient of determination (R^2) quantifies the proportion of variance in the observed data explained by the model, where a value of 1 represents a perfect prediction. The numerical formula of R^2 is given in Eq. (3).

$$R^2 = 1 - \frac{\sum_{i=1}^{n} (y_i - \hat{y_i})^2}{\sum_{i=1}^{n} (y_i - \bar{y})^2} \tag{3}$$

The optimized hyperparameter sets obtained from this procedure were subsequently used to train the final models. The selected hyperparameters and their corresponding search ranges for each model are summarized in the following **Table 7.** This standardized and systematic tuning strategy ensures that all models operate under near-optimal conditions and enables a reliable performance comparison across different ensemble learning techniques.

Table 7: Hyperparameter tuning ranges and optimal values for XGBoost

Machine Learning Technique	Hyperparameters	Range Tested
XG Boost	Learning Rate	0.01 - 0.19
	Max Depth	3 - 10
	Subsample	0.4-0.6
	Colsample Bytree	0.4-0.6
	N Estimators	50-300

In summary, to ensure accurate predictions on unseen data, the input dataset is grouped based on specimen ID and split into an 80/20 training-to-testing ratio. An XGBoost base model is trained first, followed by a hyperparameter-tuned model. After evaluating the comparisons, the highest predictive accuracy is found in the base model. Consequently, this base model is deployed to predict the continuous stress-strain curves for the unseen data. Finally, the compressive modulus and compressive stress are extracted from these predicted curves and evaluated against the actual experimental data. Figure 9 represents the workflow for machine learning modelling for the present study.

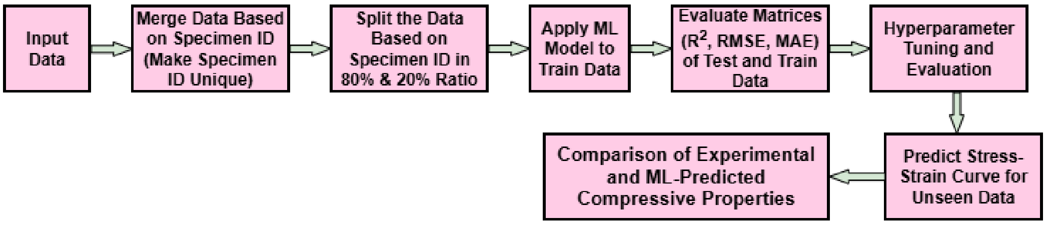

Figure 9. Workflow for machine learning modeling.

3. NEW SCIENTIFIC RESULTS – THESES

Published article related T1: REF-1

T1: Finite element analysis on polymeric lattice materials.

I investigate the compressive properties of various lattice structures by examining the effects of lattice design, filament type, and strut diameter through FEM method. These parameters are systematically analyzed to understand, optimize, and evaluate their influence on compressive behavior. FEM analysis produced satisfactory results, demonstrating strong agreement with experimental observations with 5% deviations and capturing the interactions between key parameters. The developed FEM approach provides reliable validation and predictive capability, enabling the assessment of lattice performance without the need for extensive fabrication trials. This approach reduces experimental complexity and cost while offering valuable insights for future filament development and aiding researchers in decision-making, performance evaluation, and comparative analysis of lattice structures.

1. In terms of PLA, ABS, and nylon polymers used for lattice-based structures, PLA was found to be the most suitable material, exhibiting comparatively higher effective strength 703.67 MPa and elastic modulus 2.793 GPa.
2. The SC lattice was found to be the most suitable lattice structure due to its simpler geometric design, lower manufacturing complexity, and favorable surface area compared with the FCC and SC–BCC lattice structures. The surface area of the SC lattice was determined to be approximately 7 mm^2, which contributed to its efficient structural performance and ease of fabrication.
3. The strut diameter was identified as a highly significant parameter for lattice structures, with a percentage contribution of 46.80%, demonstrating its strong influence on the mechanical properties of the lattice. The investigated strut diameter range and parameter combinations provide valuable guidelines for manufacturers in selecting appropriate design conditions to achieve improved compressive performance and optimize lattice-based applications.

Published article related T2: REF-2

T2: Experimental investigation on PLA based SC lattice structures.

I identified that the compressive properties of PLA lattice structures are highly dependent on FDM manufacturing parameters. The interactions between these parameters and the compressive performance of PLA simple cubic (SC) lattices were systematically analyzed using the Taguchi method.

1. The layer height showed highest contribution with 86.78% for compressive strngth. Moreover, this parameter is found highly significant for lattice type structure.
2. The optimized manufacturing parameters I identified for the PLA-based SC lattice structure were a layer thickness of 0.1 mm, a printing temperature of 210°C, a printing speed of 40 mm/s, and a bed temperature of 60°C.
3. A prototype lattice scaffold I developed using SC PLA structures from the optimized parameters, specifically designed for bone-related applications. This scaffold will be utilized for implantation and educational purposes, particularly in fracture-related studies. The use of PLA is advantageous due to its biocompatibility and FDA approval for certain biomedical applications.

Published article related T3: REF-3

T3: **Compressive properties and AI based performance prediction of wood-PLA SC lattice composite.**

I investigated simple cubic (SC) lattice structures fabricated using wood–PLA filament via FDM and examined the influence of manufacturing parameters on their compressive properties. The selected parameters and corresponding outcomes were analyzed using the Response Surface Methodology (RSM), which demonstrated significant interactions and strong relevance in predicting mechanical performance. Furthermore, an artificial intelligence (AI)-based framework I developed to enhance the prediction process.

1. The developed AI prediction framework demonstrated excellent predictive performance, achieving a training R^2 value of 0.999, an RMSE of 0.012, and an MAE of 0.0082, while the testing MAE was 0.1788. The proposed framework will be applied to predict the performance of wood–PLA SC lattice composites based on manufacturing parameters, thereby reducing the need for extensive fabrication and experimental testing.
2. The CatBoost prediction model achieved an error range of only 2–8.14%, demonstrating reliable predictive performance. In addition, hyperparameter tuning significantly enhanced the prediction process and improved the overall accuracy of the model, making it a robust tool for predicting the compressive behavior of wood–PLA SC lattice composites within the investigated parameter range.

Published article related T4: REF-3 and REF-4

T4: Surface analysis and performance evaluations of wood-PLA SC lattice.

An integrated validation approach was developed using Scanning Electron Microscopy (SEM) and microscopic analysis to explain the variations in mechanical properties. This approach enabled the identification of underlying reasons for both improvements and deterioration in the performance of lattice structures. Through detailed microstructural investigations, the relationship between manufacturing defects and mechanical behavior was systematically established.

1. Through microscopic and SEM analyses, I found that a higher layer height (0.3 mm), higher printing speed (60 mm/s), lower printing temperature (195°C), and 100% infill density resulted in insufficient bonding between the fibers and the matrix, as well as excessive material accumulation within the printed structures.

2. The best manufacturing outcomes with the fewest defects were achieved using a lower layer height (0.06–0.10 mm), a moderate nozzle temperature (195–205 °C), a lower printing speed (40 mm/s), and an infill density of 70%. These parameter combinations promoted improved fiber–matrix bonding, enhanced print quality, and reduced manufacturing defects in the wood–PLA SC lattice composites.

Published article related T5: REF-4

T5: Surface Chemistry Analysis of Wood–PLA SC Lattice Composites

Through a systematic investigation, I determined that manufacturing parameters significantly influence the physical properties of lattice structures, particularly for wood–PLA materials. Key properties such as contact angle, thickness swelling, and water absorption were found to be highly sensitive to processing conditions. Furthermore, the study demonstrated how and why these physical properties are closely linked to biomedical performance, especially in bone and tissue engineering applications.

1. All investigated manufacturing parameters were found to influence the surface chemistry of the wood–PLA SC lattice composites. The optimal condition was identified as DOE-27 (0.1 mm layer height, 40 mm/s printing speed, 215°C nozzle temperature, and 70% infill density), which resulted in a contact angle of 75°.

2. Among the investigated parameter combinations, DOE-27 demonstrated the lowest water absorption value of 0.91%, indicating enhanced dimensional stability and suitability for potential biomedical applications.

Published article related T6: REF-4

T6: Biomedical applications of wood-PLA SC lattice composite

I designed and proposed a scaffold for tissue engineering applications, based on the optimized outcomes of the wood–PLA lattice structures. The biological performance of the scaffold was evaluated using the TR146 cell line, where the results demonstrated that the optimized manufacturing parameters significantly enhanced cell viability, achieving approximately 98% compatibility after 7 days of exposure. Moreover, the estimated fabrication cost of the developed wood–PLA lattice scaffold is less than 1 USD, making it a highly cost-effective solution. This presents a promising alternative to conventional bone graft materials, particularly for non-load-bearing applications such as cancellous bone repair, maxillofacial and oral tissue engineering, and temporary biodegradable scaffolds.

4.LIST OF PUBLICATIONS RELATED TO THE TOPIC OF THE RESEARCH FIELD

(1) **M. M. Rahman** and J. Sultana, "Numerical and Statistical Analysis on Polymeric Lattice Structures via Taghuchi Method," 2023 International Conference on Engineering, Science and Advanced Technology (ICESAT), Mosul, Iraq, 2023, pp. 210-214, doi: 10.1109/ICESAT58213.2023.10347288.

(2) **Rahman, M.M.**, Sultana, J., Rayhan, S.B. et al. Optimization of FDM manufacturing parameters for the compressive behavior of cubic lattice cores: an experimental approach by Taguchi method. Int J Adv Manuf Technol 129, 1329–1343 (2023). https://doi.org/10.1007/s00170-023-12342-9.

(3) **Rahman MM**, Israq MA, Szávai S, Bin Rayhan S, Varga G. Experimental Characterization and a Machine Learning Framework for FDM-Fabricated Bio composite Lattice Structures. Fibers. 2026; 14(4):41. https://doi.org/10.3390/fib14040041.

(4**) Rahman MM**, Szávai S, Bin Rayhan Effect of Manufacturing Parameters on FDM-Printed Wood–PLA Lattice Composites scaffold: An In Vitro and Statistical Analysis for tissue engineering applications. (Submitted, Journal: Additive manufacturing)

(5) **Rahman MM**, Szávai S, Bin Rayhan, A current progress and application of composite and hybrid composite lattice scaffold in biomedical industries. (Submitted, Journal: Advanced composite and hybrid materials)

(6) **Rahman, Md Mazedur**, Saiaf Bin Rayhan, Jakiya Sultana, and Md Zillur Rahman. "Additive manufacturing techniques, their challenges, and additively manufactured composites for advanced engineering applications." (2024): 329-351DOI: 10.1016/B978-0-323-96020-5.00118-7.

(7) **Rahman, M.M.,** Sultana, J., Rayhan, S.B., Rahman, M.Z.: Recent advances in nanomaterials, nanocomposite and nanohybrids for biomedical and biosensing applications. In: Comprehensive Materials Processing, 2nd edn. (2024). Elsevier. https://doi.org/10.1016/B978-0-323-96020-5.00119-9.

(8) **Rahman, Md Mazedur**, and Szávai Szabolcs. "Critical Buckling and Damage Analysis of Hybrid Composite Panels with Cutouts under Uniaxial Compression Loading." Advances in Science and Technology. Trans Tech Publications Ltd, June 4, 2025. https://doi.org/10.4028/p-nji72q.

(9) **M. M. Rahman** and J. Sultana, "Design and Optimization of Natural Fiber Reinforced Hybrid Composite RVE: A Finite Element Analysis," 2023 International Conference on Engineering, Science and Advanced Technology (ICESAT), Mosul, Iraq, 2023, pp. 204-209, doi: 10.1109/ICESAT58213.2023.10347323.

(10) Khan, S., Rayhan, S. B**., Rahman, M. M**., Sultana, J., & Varga, G. (2025). Optimized ANN Model for Predicting Buckling Strength of Metallic Aerospace Panels Under Compressive Loading. Metals, 15(6), 666. https://doi.org/10.3390/met15060666.

(11) Rayhan SB, **Rahman MM**, Sultana J, Szávai S, Varga G. Finite Element and Machine Learning-Based Prediction of Buckling Strength in Additively Manufactured Lattice Stiffened Panels. Metals. 2025; 15(1):81. https://doi.org/10.3390/me

5.LITERATURE CITED IN THE THESES BOOKLET

[1] J. Sultana, S. Bin Rayhan, G. Varga, A scientometric review using CiteSpace : Progress , challenges , and applications of natural fiber-reinforced composite and hybrid composites in engineering applications (2015 – 2025), Results Eng. 28 (2025). https://doi.org/10.1016/j.rineng.2025.107670.

[2] D. Schuhmann, M. Rupp, M. Merkel, D.K. Harrison, Additive vs. Conventional Manufacturing of Metal Components: Selection of the Manufacturing Process Using the AHP Method, Processes. 10 (2022). https://doi.org/10.3390/pr10081617.

[3] M. Elbadawi, A. Basit, S. Gaisford, Energy consumption and carbon footprint of 3D printing in pharmaceutical manufacture, Int. J. Pharm. 639 (2023) 122926. https://doi.org/10.1016/j.ijpharm.2023.122926.

[4] D. Ling, D. Wang, P. Wang, X. Guo, L. Liu, B. He, L. Hu, G. Jiang, Life Cycle Assessment of 3D Printing for Precision Analytical Instrument Components: Carbon Emission Reduction Potential in ICP-MS Spray Chamber Manufacturing, ACS Sustain. Resour. Manag. 2 (2025) 1731–1741. https://doi.org/10.1021/acssusresmgt.5c00238.

[5] M.M. Rahman, S. Bin Rayhan, J. Sultana, M.Z. Rahman, Additive manufacturing techniques, their challenges, and additively manufactured composites for advanced engineering applications, 2nd ed., Elsevier Ltd., 2023. https://doi.org/10.1016/b978-0-323-96020-5.00118-7.

[6] A.H. Alami, A. Ghani Olabi, A. Alashkar, S. Alasad, H. Aljaghoub, H. Rezk, M.A. Abdelkareem, Additive manufacturing in the aerospace and automotive industries: Recent trends and role in achieving sustainable development goals, Ain Shams Eng. J. 14 (2023) 102516. https://doi.org/10.1016/j.asej.2023.102516.

[7] K. Kanishka, B. Acherjee, Revolutionizing manufacturing: A comprehensive overview of additive manufacturing processes, materials, developments, and challenges, J. Manuf. Process. 107 (2023) 574–619. https://doi.org/10.1016/j.jmapro.2023.10.024.

[8] M.M. Rahman, J. Sultana, S. Bin Rayhan, A. Ahmed, Optimization of FDM manufacturing parameters for the compressive behavior of cubic lattice cores: an experimental approach by Taguchi method, Int. J. Adv. Manuf. Technol. 129 (2023) 1329–1343. https://doi.org/10.1007/s00170-023-12342-9.

[9] G. veiw Reserach, U.S. Additive Manufacturing Market (2023 - 2030), 2022. https://www.grandviewresearch.com/industry-analysis/us-additive-manufacturing-market-report.

[10] P. Research, Additive Manufacturing Market Revenue, Top Companies, Report 2033, Preced. Res. (2022). https://www.precedenceresearch.com/press-release/additive-manufacturing-market.

[11] and M.M. Fares Mami, Jean-Pierre Rev´eret, Sophie Fallaha, Evaluating Eco-Efficiency of 3D Printing in the Aeronautic Industry, J. Ind. Ecol. 21 (2017). https://doi.org/DOI: 10.1111/jiec.12693.

[12] W. Zhang, X. Zhang, H.Y. Chong, J. Li, Carbon Emission Insights From a Real 3D Printed Bus Station, Adv. Civ. Eng. 2025 (2025). https://doi.org/10.1155/adce/6743618.

[13] S. Zakaria, P. Mativenga, A scientific base for optimising energy consumption and performance in 3D printing, J. Clean. Prod. 482 (2024) 144227. https://doi.org/10.1016/j.jclepro.2024.144227.

[14] C. Pan, Y. Han, J. Lu, Design and optimization of lattice structures: A review, Appl. Sci. 10 (2020) 1–36. https://doi.org/10.3390/APP10186374.

[15] S. Bin Rayhan, M.M. Rahman, J. Sultana, S. Szávai, G. Varga, Finite Element and Machine Learning-Based Prediction of Buckling Strength in Additively Manufactured Lattice Stiffened Panels, Metals (Basel). 15 (2025) 1–18. https://doi.org/10.3390/met15010081.

[16] D. Mahmoud, M.A. Elbestawi, Lattice structures and functionally graded materials applications in additive manufacturing of orthopedic implants: A review, J. Manuf. Mater. Process. 1 (2017) 1–19. https://doi.org/10.3390/jmmp1020013.

[17] M.A. El-Sayed, K. Essa, M. Ghazy, H. Hassanin, Design optimization of additively manufactured titanium lattice structures for biomedical implants, Int. J. Adv. Manuf. Technol. 110 (2020) 2257–2268. https://doi.org/10.1007/s00170-020-05982-8.

[18] Q. Shi, J. Chen, J. Chen, Y. Liu, H. Wang, Application of additively manufactured bone scaffold: a systematic review, Biofabrication. 16 (2024). https://doi.org/10.1088/1758-5090/ad35e8.

[19] N. Sultana, Mechanical and biological properties of scaffold materials, Elsevier Ltd, 2018. https://doi.org/10.1016/B978-0-08-100979-6.00001-X.

[20] S. Polo, A. García-Domínguez, E.M. Rubio, J. Claver, Lattice Structures in Additive Manufacturing for Biomedical Applications: A Systematic Review, Polymers (Basel). 17 (2025). https://doi.org/10.3390/polym17172285.

[21] X. Yue, J. Shang, M. Zhang, B. Hur, X. Ma, Additive manufacturing of high porosity magnesium scaffolds with lattice structure and random structure, Mater. Sci. Eng. A. 859 (2022) 144167. https://doi.org/10.1016/j.msea.2022.144167.

[22] J. Hulme, A.H. Sakhaei, M. Shafiee, Mechanical analysis and additive manufacturing of 3D-printed lattice materials for bone scaffolds, Procedia Struct. Integr. 63 (2024) 30–37. https://doi.org/10.1016/j.matpr.2023.02.278.

[23] B.I. Oladapo, S.O. Ismail, A. V. Adebiyi, F.T. Omigbodun, M.A. Olawumi, D.B. Olawade, Nanostructural interface and strength of polymer composite scaffolds applied to intervertebral bone, Colloids Surfaces A Physicochem. Eng. Asp. 627 (2021) 127190. https://doi.org/10.1016/j.colsurfa.2021.127190.

[24] S. Murchio, M. Benedetti, A. Berto, F. Agostinacchio, G. Zappini, D. Maniglio, Hybrid Ti6Al4V/Silk Fibroin Composite for Load-Bearing Implants: A Hierarchical Multifunctional Cellular Scaffold, Materials (Basel). 15 (2022). https://doi.org/10.3390/ma15176156.

[25] M. Mahmoudi, M. Dargahi, S. Mashayekhan, R. Jahanmardi, H. Baniasadi, Structure–property–function relationships in 3D-printed gelatin/cellulose nanocrystals/n-HAP scaffolds for bone tissue repair, Int. J. Biol. Macromol. 328 (2025) 147790. https://doi.org/10.1016/j.ijbiomac.2025.147790.

[26] R. McMullan, A. Golbang, K. Salma-Ancane, J. Ward, K. Rodzen, A.R. Boyd, Review of 3D Printing of Polyaryletherketone/Apatite Composites for Lattice Structures for Orthopedic Implants, Appl. Sci. 15 (2025) 1–28. https://doi.org/10.3390/app15041804.

[27] K.K. Alaneme, S.A. Kareem, J.L. Olajide, R.E. Sadiku, M.O. Bodunrin, Computational biomechanical and biodegradation integrity assessment of Mg-based biomedical devices for cardiovascular and orthopedic applications: A review, Int. J. Light. Mater. Manuf. 5 (2022) 251–266. https://doi.org/10.1016/j.ijlmm.2022.02.003.

[28] Y. Wang, J. Sultana, M.M. Rahman, A. Ahmed, A. Azam, R.T. Mushtaq, M. Rehman,

A Sustainable and Biodegradable Building Block: Review on Mechanical Properties of Bamboo Fibre Reinforced PLA Polymer Composites and Their Emerging Applications, Fibers Polym. 23 (2022) 3317–3342. https://doi.org/10.1007/s12221-022-4871-z.

[29] B.I. Oladapo, S.A. Zahedi, S.O. Ismail, F.T. Omigbodun, O.K. Bowoto, M.A. Olawumi, M.A. Muhammad, 3D printing of PEEK–cHAp scaffold for medical bone implant, Bio-Design Manuf. 4 (2021) 44–59. https://doi.org/10.1007/s42242-020-00098-0.

[30] W. Wang, L. Wang, B. Zhang, S. Shang, C. Zhao, W. Zhang, J. Chen, C. Zhou, H. Zhou, S. Feng, 3D printing of personalized magnesium composite bone tissue engineering scaffold for bone and angiogenesis regeneration, Chem. Eng. J. 484 (2024) 149444. https://doi.org/10.1016/j.cej.2024.149444.

[31] M. Kaur, T.G. Yun, S.M. Han, E.L. Thomas, W.S. Kim, 3D printed stretching-dominated micro-trusses, Mater. Des. 134 (2017) 272–280. https://doi.org/10.1016/j.matdes.2017.08.061.

[32] T.A. Alwattar, A. Mian, Development of an elastic material model for bcc lattice cell structures using finite element analysis and neural networks approaches, J. Compos. Sci. 3 (2019). https://doi.org/10.3390/jcs3020033.

[33] C. Peng, P. Tran, H. Nguyen-Xuan, A.J.M. Ferreira, Mechanical performance and fatigue life prediction of lattice structures: Parametric computational approach, Compos. Struct. 235 (2020) 111821. https://doi.org/10.1016/j.compstruct.2019.111821.

[34] N. Jin, F. Wang, Y. Wang, B. Zhang, H. Cheng, H. Zhang, Effect of structural parameters on mechanical properties of Pyramidal Kagome lattice material under impact loading, Int. J. Impact Eng. 132 (2019). https://doi.org/10.1016/j.ijimpeng.2019.06.002.

[35] N. Dixit, P.K. Jain, Effect of Fused Filament Fabrication Process Parameters on Compressive Strength of Thermoplastic Polyurethane and Polylactic Acid Lattice Structures, J. Mater. Eng. Perform. 31 (2022) 5973–5982. https://doi.org/10.1007/s11665-022-06664-0.

[36] M.R. Karamooz Ravari, M. Kadkhodaei, M. Badrossamay, R. Rezaei, Numerical investigation on mechanical properties of cellular lattice structures fabricated by fused deposition modeling, Int. J. Mech. Sci. 88 (2014) 154–161. https://doi.org/10.1016/j.ijmecsci.2014.08.009.

[37] R.A. Hamid, F.H. Hamezah, J. Abd Razak, Influence of Humidity on the Tensile Strength of 3D Printed PLA Filament, Springer Singapore, 2022. https://doi.org/10.1007/978-981-16-8954-3_47.

[38] M. Algarni, The influence of raster angle and moisture content on the mechanical properties of pla parts produced by fused deposition modeling, Polymers (Basel). 13 (2021) 1–12. https://doi.org/10.3390/polym13020237.

[39] A.K. Mishra, H. Chavan, A. Kumar, Effect of material variation on the uniaxial compression behavior of FDM manufactured polymeric TPMS lattice materials, Mater. Today Proc. 46 (2021) 7752–7759. https://doi.org/10.1016/j.matpr.2021.02.276.

[40] C. Tang, J. Liu, Y. Yang, Y. Liu, S. Jiang, W. Hao, Effect of process parameters on mechanical properties of 3D printed PLA lattice structures, Compos. Part C Open Access. 3 (2020). https://doi.org/10.1016/j.jcomc.2020.100076.

[41] R.G. Silva, C.S. Estay, G.M. Pavez, J.Z. Viñuela, M.J. Torres, Influence of geometric and manufacturing parameters on the compressive behavior of 3d printed polymer

lattice structures, Materials (Basel). 14 (2021). https://doi.org/10.3390/ma14061462.
[42] Qidi, Qidi-PLA wood filament, (n.d.). https://eu.qidi3d.com/products/pla-wood-filament (accessed February 11, 2026).
[43] M. Kariz, M. Sernek, M.K. Kuzman, E ffect of wood content in FDM fi lament on properties of 3D printed parts, Mater. Today. 14 (2018) 135–140. https://doi.org/10.1016/j.mtcomm.2017.12.016.
[44] M.K. Poddar, R. Kumar, S.K. Sarangi, Optimizing FDM 3D printing parameters for enhanced compressive strength in PLA fluorite lattice structures : a Taguchi design and finite element analysis approach Optimizing FDM 3D printing parameters for enhanced compressive strength in PLA fluorite latt, Eng. Res. Express. 7 (2025).
[45] M.K. Poddar, R. Kumar, S.K. Sarangi, Optimizing FDM 3D printing parameters for enhanced compressive strength in PLA fluorite lattice structures : a Taguchi design and finite element analysis approach, Eng. Res. Express. 7 (2025) 045556.
[46] C. Tang, J. Liu, Y. Yang, Y. Liu, S. Jiang, W. Hao, Effect of process parameters on mechanical properties of 3D printed PLA lattice structures, Compos. Part C Open Access. 3 (2020) 1–14. https://doi.org/10.1016/j.jcomc.2020.100076.
[47] P. Lohmuller, J. Favre, P. Laheurte, Stress Concentration and Mechanical Strength of Cubic Lattice Architectures, Materials (Basel). 11 (2018) 1–12. https://doi.org/10.3390/ma11071146.
[48] K. Park, K. Min, Y. Roh, Design Optimization of Lattice Structures under Compression : Study of Unit Cell Types and Cell Arrangements, Materials (Basel). 15 (2022). https://doi.org/https://doi.org/10.3390/ma15010097.
[49] V. Mahesh, ANN based prediction of the absorption characteristics of additive manufactured glycol-modified polyethylene terephthalate nanocomposites reinforced with short-carbon fibers and nanoclay fillers, Polym. Compos. 44 (2023) 8223–8239. https://doi.org/10.1002/pc.27337.
[50] M.A. Alsmael, S.W. Ibrahim, M.H.M. Alsharbaty, S.S. Ali, M. Schagerl, Enhanced Mechanical and Surface Performance of Three-Dimensionally Printed Denture Base Resin via Zinc Oxide and Samarium Oxide Nanoparticle Reinforcement, Materials (Basel). 19 (2026) 1–25.
[51] G. Repetto, A. Peso, J.L. Zurita, Neutral red uptake assay for the estimation of cell viability / cytotoxicity, Nature. 3 (2008) 1125–1131. https://doi.org/10.1038/nprot.2008.75.
[52] Ensemble learning, (2026). https://www.academia.edu/2813351/Ensemble_learning (accessed January 9, 2026).
[53] M. Rahman, A. Israq, S. Szávai, S. Bin Rayhan, G. Varga, Experimental Characterization and a Machine Learning Framework for FDM-Fabricated Biocomposite Lattice Structures, Fibers. (2026) 1–25.